Quadruple coincidence measurement of electron correlation in strong-field molecular double ionization

Arthur Zhao,[1] Chuan Cheng,[1] Spiridoula Matsika,[2] and Thomas Weinacht[1]
[1]*Department of Physics and Astronomy, Stony Brook University, Stony Brook, New York 11794-3800, USA*
[2]*Department of Chemistry, Temple University, Philadelphia, Pennsylvania 19122, USA*

(Received 16 February 2018; published 12 April 2018)

We study strong-field dissociative molecular double ionization with momentum-resolved quadruple coincidence measurements, measuring the two electrons and two ionic fragments produced with a coincidence velocity map imaging apparatus. We contrast measurements for two different molecules. In one case, our measurements reveal anticorrelation in the momentum for the two electrons. In the other, we find no anticorrelation, indicating differences in the underlying ionization dynamics.

DOI: 10.1103/PhysRevA.97.043412

I. INTRODUCTION

Strong-field double ionization (DI) has been the focus of many investigations over the past three decades [1–19] (see [20–22] for reviews). In particular, nonsequential double ionization (NSDI) in an intense laser field has been of great interest since it directly probes electron correlations. As a result of particle correlations and nonperturbative field interaction, one can no longer invoke the single-electron approximation (SEA) [23]. This makes theoretical modeling difficult. To date, most efforts have been focused on the DI of rare-gas atoms where most observations can be well explained by a simple semiclassical rescattering model [5,24]. In this model, one electron is first liberated near the peak of the field and then accelerated back by the alternating field to collide with the ion. With sufficient energy, it can directly knock out a second electron, resulting in an $(e,2e)$ scattering event. If the energy is below the second ionization potential, inelastic scattering can excite a second electron which is later field ionized. This second case is termed recollision excitation with subsequent ionization (RESI) [16,25–27]. Momentum-resolved coincidence measurements which yield electron joint momentum distributions (EJMDs) [28] can help distinguish between recollision-driven excitation vs ionization.

The situation with molecules is more complicated and the ionization dynamics are not understood as well. A few studies have considered strong-field DI of molecules [28–36], but there are very few momentum-resolved coincidence measurements [37,38] and no general framework for understanding the dynamics. Unlike rare-gas atoms, molecules have a richer electronic structure which can play a significant role during NSDI. The valence electrons in molecules that form molecular bonds have the lowest ionization potentials. They are delocalized over two or more nuclei and tend to have a larger spatial extent compared with electrons in atoms. This can complicate the rescattering process since the scattering potential has a more structured landscape compared to an atom. In addition, due to the larger spatial extent, when the first electron is liberated from a valence bond, it is more likely to scatter off other electrons on its way out. This can result in a "shake-off" process, which has been previously proposed to explain NSDI in atoms [4].

In a previous study, we observed enhanced DI yields in 1,3-cyclohexadiene (CHD, C_6H_8) and 1,3-butadiene (C_4H_6) (both conjugated systems, with alternating single and double molecular bonds), which was not found in two nonconjugated molecules: cyclohexane (C_6H_{12}) and cyclopentane (C_5H_{10}) [39]. Our measurements (including intensity-dependent measurements of the DI yield) indicated that DI takes place before the saturation of single ionization, and hence is nonsequential. Here we present a further study of the dissociative double ionization (DDI) of CHD with momentum-resolved quadruple coincidence (two ions and two electrons) measurements. The main goals of this present study are (1) to illustrate the apparatus' ability to record momentum-resolved quadruple coincidences, which is technically challenging, and, more importantly, (2) to describe the observation of distinct correlations in the joint electron momentum distributions for electrons coming from different dissociation channels during double ionization. We report an interesting observation of dissociation-channel-specific EJMD. For one channel, we see a statistically significant anticorrelation in the momenta for the two electrons. We argue that if the dissociation channel is determined by the state of the dication after both electrons are removed, then the channel-specific EJMD provides information on which molecular orbitals participate in the DDI.

II. EXPERIMENT AND RESULTS

We make use of a recently developed apparatus for coincidence, which has been described in detail in an earlier publication [40]. Briefly, using a Ti:sapphire amplifier in conjunction with filament-based spectral broadening and grating compression [41], we generate 9 fs (FWHM intensity) pulses at 1 kHz, centered around 750 nm. The laser pulses are focused into an effusive molecular beam in a velocity map imaging (VMI) apparatus (Fig. 1), which maps the transverse momentum of a charged particle onto the position of the detector [42]. By switching the voltages on the VMI plates using two DEI Scientific pulse generators (<25 ns rise or fall time), in sync with the arrival of the laser pulse, we collect both electrons and ions for each laser shot with a single detector.

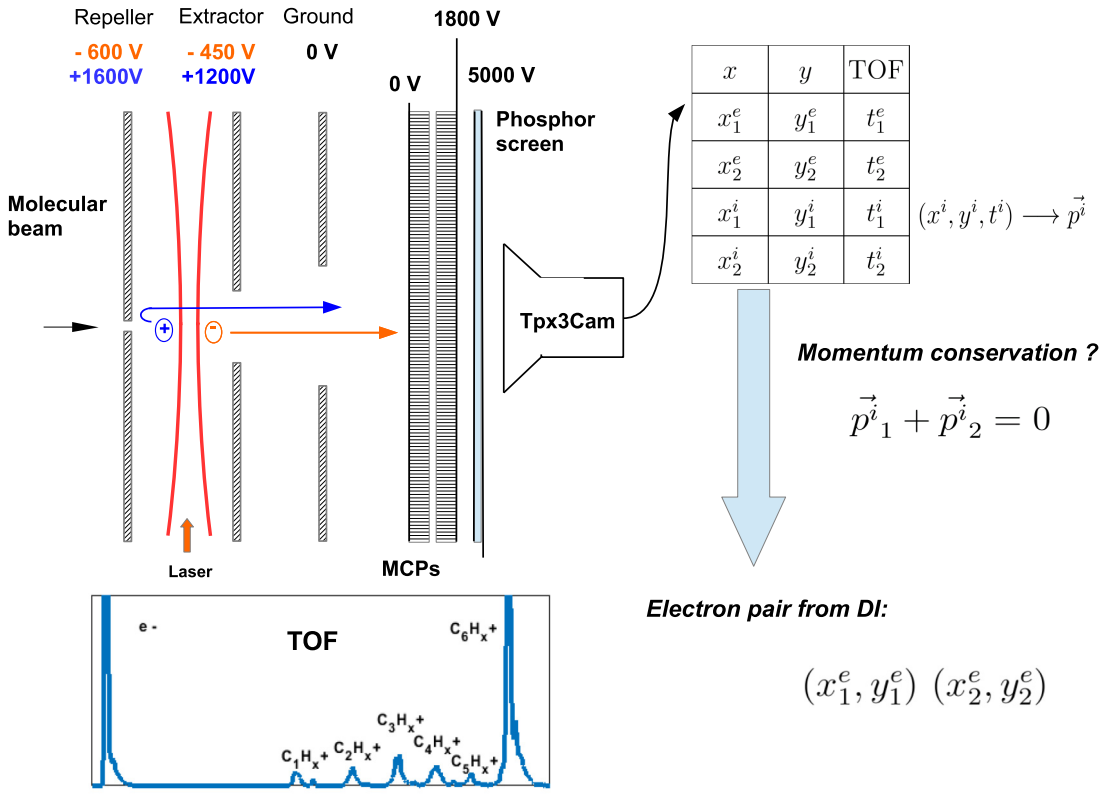

FIG. 1. Coincidence velocity map imaging (VMI) apparatus. Voltages on the VMI plates (repeller and extractor) are switched to collect both electrons and ions generated from each laser shot. A time-stamping camera records all active pixels (signal above a threshold) as a list of x, y and time of flight (TOF). For ions, the 1.5 ns resolution allows the conversion from TOF to momentum in the z direction, which, together with the spatial information (x, y), allows for the recovery of 3D momenta. We use this information to check if the two detected ions conserve momentum and thus originate from a single molecule. Two electrons detected in coincidence with a pair of momentum-conserving ions are considered as coming from a DI event.

When the laser pulse interacts with the molecules, the voltages on the VMI plates are initially negative, allowing for the collection of electrons. After the electrons leave the interaction region, the voltages are switched to positive values, allowing for the collection of positively charged ions. The detector consists of a dual stack of microchannel plates (MCPs), a phosphor screen, and a Tpx3Cam camera, which is a novel time-stamping optical camera with 1.5 ns resolution [43]. Compared to a conventional cold target recoil ion momentum spectroscopy (COLTRIMS) apparatus [28,44], this camera-based detector is much simpler and can easily detect a relatively large number of charged particles directly, which is well suited to many-particle coincidence measurements. Using a centroiding algorithm, we first identify hits on the camera and save their position and time of flight (TOF) in the format of (x,y,t). Then we convert the TOF of an ion to its longitudinal momentum and subsequently recover its three-dimensional (3D) momentum. Finally, for each laser shot, we check if (1) there are exactly two ion fragments which constitute the whole molecule (e.g., $C_2H_4^+$ and $C_4H_4^+$ from C_6H_8) which (2) conserve momentum, and (3) there are exactly two electrons. If so, we consider the two electrons measured in coincidence with these two ion fragments as coming from one DDI event. The measurement of two fragments whose combined mass equals the parent ion mass and conserve momentum provides a very strong constraint which effectively restricts us to only DDI events. Under this constraint, the dominant contribution to false coincidences comes from the scenario where an additional single-ionization event occurs, whose ion is not detected and whose electron is detected instead of one of the electrons from the DDI event. Based upon our average number of single- and double-ionization events per shot (~0.5) and our detection efficiencies for electrons and ions (50% and 30%, respectively), we estimate the false-coincidence contributions to our data to be about 20% or less (see the Appendix for a detailed discussion). Since false coincidences will tend to decrease any correlations in the EJMD, the actual correlations or anticorrelations are a little stronger than we observe in our measurements [45].

Having measured the momentum of electron pairs resulting from DDI, we can plot the momentum of one electron vs the other, either parallel or perpendicular to the laser polarization. We consider electrons coming from three main fragmentation channels for doubly ionized 1,3-cyclohexadiene (CHD, C_6H_8): C_1C_5 ($C_1H_x^+$, $C_5H_x^+$), C_2C_4 ($C_2H_x^+$, $C_4H_x^+$), and C_3C_3 ($C_3H_x^+$, $C_3H_x^+$). The subscript x indicates an unspecified number of hydrogens since we do not discriminate between fragments with the same number of carbons but different hydrogens. Figure 2 shows the 2D raw images for ions [Fig. 2(a)] and electrons [Fig. 2(c)] along with their 3D joint momentum distributions [Figs. 2(b) and 2(d)] for the ($C_1H_x^+$, $C_5H_x^+$) channel. The raw images show a cumulative

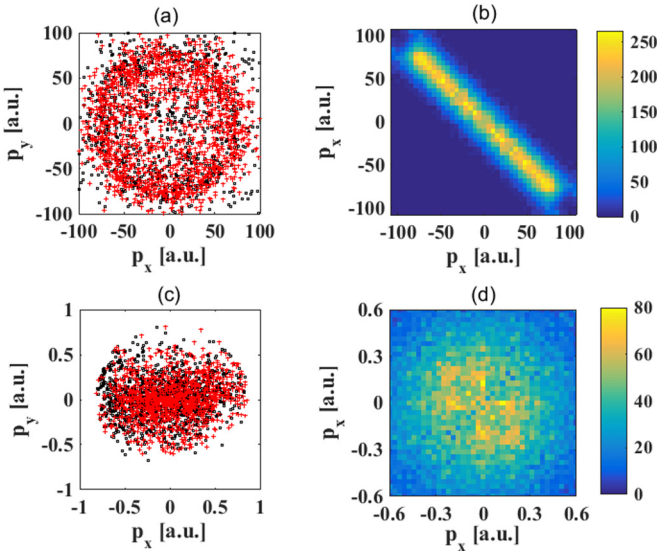

FIG. 2. (a) Momentum distributions of momentum-conserving ion pair ($C_1H_x^+$, $C_5H_x^+$) and (c) their corresponding electrons. (b) The joint momentum distribution (JMD) for (a), which exhibits an anticorrelation as expected from momentum conservation. (d) The JMD for (c), which shows small but nontrivial anticorrelation.

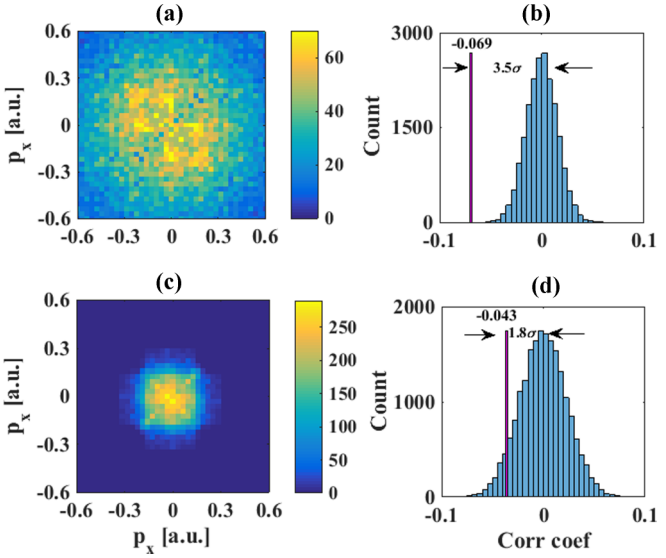

FIG. 3. Comparison of EJMD from two molecules: (a) C_6H_8 and (c) CH_2IBr. By randomizing the pairing of the two electrons, we can generate histograms (b) C_6H_8 and (d) CH_2IBr, showing the statistical significance of the anticorrelation quantified by the r_P (corr coef). The y axis labels the number of random pairings. Fitting the histogram with a Gaussian distribution, the observed correlation coefficient in C_6H_8 is 3.5 σ away from the mean 0, with a p value of 0.0003. In contrast, we see a smaller correlation in the EJMD for CH_2IBr, with a p value of just over 0.05.

momentum distribution of particles coming from laser shots which generate exactly two ions and two electrons. We show in red those ion pairs that conserve momentum and their corresponding electrons. In Fig. 2(a), there is a clear ring in which the majority of the momentum-conserved ion fragments fall. This is consistent with the anticorrelation observed in panel (a) and the fact that momentum-conserving $C_1H_x^+$ and $C_5H_x^+$ fragments have equal and opposite momentum. More interestingly, the well-defined kinetic-energy release implies that most fragments come from a single (or several closely spaced) excited dicationic state(s) (the ground state of the dication is nondissociative). In addition, the isotropy of the distribution suggests that the ionization is not sensitive to the laser polarization, given that the measurements are performed with linearly polarized laser pulses. This ion ring coming from DDI has been observed before [39], and the fact that it is observed for some molecules and not others suggests that the DDI mechanism depends on the specific electronic structure of the molecule (e.g., conjugation). This motivates the study of the EJMD, shown in Fig. 2(d). The anticorrelation observed in the EJMD implies that for the C_1C_5 fragmentation channel, the two liberated electrons tend to fly away from each other.

In order to quantify this anticorrelation, we calculate the Pearson correlation coefficient (r_P) [46], also known as the normalized correlation coefficient, between the momenta of two electrons along the laser polarization direction (p_{x1} and p_{x2}):

$$r_P(p_{x1},p_{x2}) = \frac{\mathrm{cov}(p_{x1},p_{x2})}{\sigma(p_{x1})\sigma(p_{x2})}, \tag{1}$$

where cov is the covariance and σ is the standard deviation (we discuss more details of the r_P calculation in Fig. 4 and the surrounding text). The r_P measures the amount of linear correlation between two variables and takes on a continuous value between -1 and $+1$. A $r_P = \pm 1$ implies perfect correlation or anticorrelation, respectively. $r_P = 0$ implies no correlation, that is, the two variables are independent. For electrons measured in the C_1C_5 channel, their momenta along the laser-polarization direction has a $r_P = -0.069$. The null hypothesis (i.e., no correlation) corresponds to $r_P = 0$. To quantify the statistical significance of this observation, we generate a statistical distribution based on the data by randomizing the pairing of the electrons from different laser shots. More precisely, starting with the list of (p_{x1}, p_{x2}) obtained from coincidence measurement, we fix the ordering of p_{x1} while randomly permute the ordering of p_{x2} and calculate the r_P for the new pairing. Figure 3(b) shows the histogram of r_P generated by 20 000 random pairings and the r_P of the real data. Assuming the null hypothesis follows a Gaussian distribution [i.e., fitting the histogram in Fig. 3(b) to a Gaussian], a $r_P = -0.069$ corresponds to a 3.5 σ observation. In comparison, the EJMD for bromoiodomethane, CH_2IBr, associated with the CH_2Br^+ and I^+ channels [Figs. 3(c) and 3(d)] show a smaller correlation. This comparison indicates that the anticorrelation we observe in EJMD for the C_1C_5 channel of C_6H_8 is not due to a systematic error in our apparatus or analysis protocol, and shows there are indeed interesting dynamics during the DI of C_6H_8. We also calculate the p value, which is a statistical measure of how significant an observation is [47]. The smaller the p value, the less likely the observation is random. Using 1 000 000 random pairings, we calculate a p value of 0.0003 for the C_1C_5 channel of C_6H_8 (in this case, 0.0003 is the area under the Gaussian curve that is outside of $r_P = \pm 0.069$) for C_6H_8, much less than the commonly used threshold of 1%. A similar calculation of the p value for the electrons in coincidence

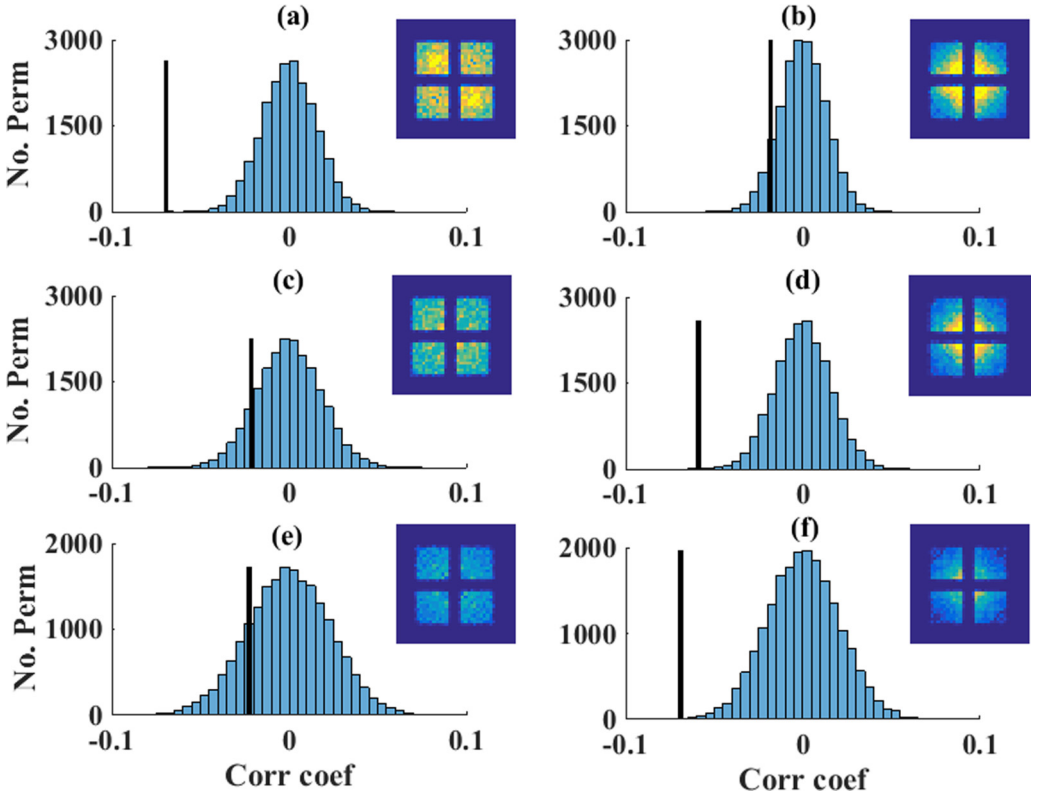

FIG. 4. Pearson correlation coefficient (r_P) and electron joint momentum distribution (EJMD) for all fragmentation channels in C_6H_8. The r_P for electrons originating from the same molecule are indicated by the dark vertical bar, and the r_P for randomly paired electrons are displayed in terms of a histogram with lightly shaded bars. The x axis is the r_P and the y axis is the number of permutations or pairings. All histograms contains 20 000 random pairings. (a) $p_x - p_x$ in the C_1C_5 channel, with x being the direction of laser polarization. (b) $p_y - p_y$ in the C_1C_5 channel. (c) $p_x - p_x$ in the C_2C_4 channel. (d) $p_y - p_y$ in the C_2C_4 channel. (e) $p_x - p_x$ in the C_3C_3 channel. (f) $p_y - p_y$ in the C_3C_3 channel. The scales for the six EJMD insets are similar to those in Fig. 3, but with different ranges: (a),(c),(e) [0 60] and (b),(d),(f) [0 100].

with the I^+ and CH_2Br^+ fragments from CH_2IBr yields just over 0.05. This further confirms the statistical significance of the measured anticorrelation in C_6H_8, and motivates the idea that molecular DDI depends on the electronic structure of the molecule.

Here we explain the details of how we calculate the r_P and further examine the EJMD for various dissociation channels. Since C_6H_8 shows an enhanced DI yield, and coincidence measurements of DI usually suffers from low statistics, we focus on the results for C_6H_8. In addition to the anticorrelation shown in the EJMD in Fig. 3(a), we see that there are large populations of electrons distributed around the x and y axis. These electrons may result from RESI where the second electron is first excited by the recolliding electron and then tunnels to the continuum with minimal energy near the peak of a subsequent half cycle. This is a generic feature which we have observed in all fragmentation channels and for both molecules. On the other hand, it is likely that there is more than one mechanism at play, and the resulting electrons have different momentum distributions. Momentum-resolved coincidence measurements allow for a highly differential study of the EJMD. In order to take advantage of this, we set up two simple momentum filters to cut out low- (around zero) and high-momentum electrons for the calculation of the r_P. An additional criterion is to include as many electrons as possible for good statistics. The passing band is set to be between 0.06 and 0.37 a.u. momentum, which is optimized for the C_1C_5 channel. Figure 4 shows the r_P and a histogram obtained from random pairing for each fragmentation channel for C_6H_8, both parallel and perpendicular to the laser-polarization directions, similar to Fig. 3(b). The corresponding EJMDs for each channel and direction are shown as insets. All EJMDs have the same range as Fig. 3(a). By comparing the inset in Fig. 4(a) with Fig. 3(a), one can see exactly where the cuts are set. Note that in Fig. 3, the calculated r_P are based on the filtered EJMD, even though we show the whole momentum range in the EJMD.

Figure 4 shows that in the above-mentioned momentum range, electron momenta along the laser polarization measured in the C_1C_5 channel have a significant anticorrelation, which is absent in the other two channels. Based on the kinetic-energy release in Fig. 2(a) (or [39]), we know that the fragments come from a high-lying dissociative state of the dicaton, and that this involves the removal of deeply bound electrons (i.e., the two electrons cannot both come from the highest occupied molecular orbital). If the first electron interacts with the second electron in different ways depending on the orbital from which the second electron is removed, and the creation of an electron hole in different orbitals is correlated with different fragmentation channels, then we would expect a correlation

between the EJMD and dissociation channel, i.e., different EJMD for different fragments. This suggests that the electronic structure of the molecule could play an important role in DDI. We also observe an anticorrelation perpendicular to the laser polarization [Figs. 4(b), 4(d) and 4(f)]. However, we note that in this case since the majority of data points are located near the center (see Fig. 3), which is excluded from the calculation, the r_P is calculated with lower statistics and should thus be interpreted with caution.

III. CONCLUSION

In conclusion, we have carried out momentum-resolved measurements of strong-field molecular double ionization. By detecting all four resulting particles in coincidence, we observe an anticorrelation in the EJMD of C_6H_8, for a particular dissociation channel within a specific momentum range, and a lack of correlation in the case of CH_2IBr. A detailed analysis of the correlation statistics helps establish the significance of the anticorrelation and rule out systematic issues. The measurements show that the EJMDs for electrons associated with different dissociation channels are distinct, indicating that the correlated electron dynamics involved in producing different fragments are different. Since different dissociation channels involved different molecular orbitals, our measurements indicate that the electron correlation involved in molecular double ionization depends on the orbitals involved. We are currently working on calculations to interpret the measurements in detail.

ACKNOWLEDGMENTS

We gratefully acknowledge support from the US Department of Energy under Awards No. DE-FG02-08ER15983 and No. DE-FG02-08ER15984.

APPENDIX: FALSE-COINCIDENCE ESTIMATION

Here we discuss the coincidence probability and the leading false coincidence. We assume both single ionization (SI) and double ionization (DI) follow Poisson distribution, with independent mean $\lambda = \lambda_1$ for SI and $\lambda = \lambda_2$ for DI. n is the number of SI or DI events:

$$P(n) = \frac{\lambda^n}{n!} e^{-\lambda}. \tag{A1}$$

Further assume that the detection efficiencies are a and b for the electron and ion, respectively. Then, for SI, the probability of detecting α electrons and β ions is

$$\begin{aligned} P_1(\alpha,\beta) &= \Sigma_n P_1(n)\, C_n^\alpha (1-a)^{n-\alpha} a^\alpha C_n^\beta (1-b)^{n-\beta} b^\beta \\ &= \left(\frac{a}{1-a}\right)^\alpha \left(\frac{b}{1-b}\right)^\beta \Sigma_n P_1(n)\, C_n^\alpha C_n^\beta \\ &\quad \times (1-a)^n (1-b)^n, \end{aligned} \tag{A2}$$

where $C_n^\alpha = n!/[\alpha!(n-\alpha)!]$. Similarly, for DI, the probability is

$$\begin{aligned} P_2(\alpha,\beta) &= \Sigma_m P_2(m)\, C_{2m}^\alpha (1-a)^{2m-\alpha} a^\alpha C_{2m}^\beta (1-b)^{2m-\beta} b^\beta \\ &= \left(\frac{a}{1-a}\right)^\alpha \left(\frac{b}{1-b}\right)^\beta \Sigma_m P_2(m)\, C_{2m}^\alpha C_{2m}^\beta \\ &\quad \times (1-a)^{2m} (1-b)^{2m}. \end{aligned} \tag{A3}$$

However, $P_2(2,2)$ contains both true and false coincidences because the two electrons and two ions may not come from the same molecule. Considering only the true coincidence contribution, we have

$$\begin{aligned} P_{\text{true}} &= P_1(0,0) P_{2,\text{true}}(2,2) \\ &= C_1 C_2 \lambda_2 a^2 b^2, \end{aligned} \tag{A4}$$

where $C_1 = e^{-\lambda_1 + \lambda_1 (1-a)(1-b)}$ and $C_2 = e^{-\lambda_2 + \lambda_2 (1-a)^2 (1-b)^2}$.

Among all the false-coincidence events, the leading contribution is the case when one electron from an SI event is detected together with one electron and two ions from the same DI event. The case when two ions come from different molecules is largely filtered out by the momentum-conservation filter. Thus,

$$\begin{aligned} P_{\text{leading false}} &= C_1 C_2\, 2\, \lambda_1 \lambda_2 (1-a)(1-b) a^2 b^2 \\ &= 2\lambda_1 (1-a)(1-b)\, P_{\text{true}}. \end{aligned} \tag{A5}$$

[1] A. L'Huillier, L. A. Lompre, G. Mainfray, and C. Manus, Phys. Rev. Lett. **48**, 1814 (1982).

[2] D. Feldmann, J. Krautwald, S. Chin, A. Von Hellfeld, and K. Welge, J. Phys. B **15**, 1663 (1982).

[3] M. Y. Kuchiev, JETP Lett. **45**, 404 (1987).

[4] D. N. Fittinghoff, P. R. Bolton, B. Chang, and K. C. Kulander, Phys. Rev. Lett. **69**, 2642 (1992).

[5] P. B. Corkum, Phys. Rev. Lett. **71**, 1994 (1993).

[6] B. Walker, B. Sheehy, L. F. DiMauro, P. Agostini, K. J. Schafer, and K. C. Kulander, Phys. Rev. Lett. **73**, 1227 (1994).

[7] A. Talebpour, S. Larochelle, and S.-L. Chin, J. Phys. B **30**, L245 (1997).

[8] S. Larochelle, A. Talebpour, and S.-L. Chin, J. Phys. B **31**, 1201 (1998).

[9] R. Moshammer, B. Feuerstein, W. Schmitt, A. Dorn, C. D. Schröter, J. Ullrich, H. Rottke, C. Trump, M. Wittmann, G. Korn *et al.*, Phys. Rev. Lett. **84**, 447 (2000).

[10] T. Weber, H. Giessen, M. Weckenbrock, G. Urbasch, A. Staudte, L. Spielberger, O. Jagutzki, V. Mergel, M. Vollmer, and R. Dörner, Nature (London) **405**, 658 (2000).

[11] G. L. Yudin and M. Y. Ivanov, Phys. Rev. A **63**, 033404 (2001).

[12] A. Rudenko, K. Zrost, B. Feuerstein, V. L. B. De Jesus, C. D. Schröter, R. Moshammer, and J. Ullrich, Phys. Rev. Lett. **93**, 253001 (2004).

[13] V. B. de Jesus, B. Feuerstein, K. Zrost, D. Fischer, A. Rudenko, F. Afaneh, C. D. Schröter, R. Moshammer, and J. Ullrich, J. Phys. B **37**, L161 (2004).

[14] J. Rudati, J. L. Chaloupka, P. Agostini, K. C. Kulander, and L. F. DiMauro, Phys. Rev. Lett. **92**, 203001 (2004).

[15] M. Weckenbrock, D. Zeidler, A. Staudte, T. Weber, M. Schöffler, M. Meckel, S. Kammer, M. Smolarski, O. Jagutzki, V. R. Bhardwaj *et al.*, Phys. Rev. Lett. **92**, 213002 (2004).
[16] S. L. Haan, L. Breen, A. Karim, and J. H. Eberly, Phys. Rev. Lett. **97**, 103008 (2006).
[17] B. Bergues, M. Kübel, N. G. Johnson, B. Fischer, N. Camus, K. J. Betsch, O. Herrwerth, A. Senftleben, A. M. Sayler, T. Rathje *et al.*, Nat. Commun. **3**, 813 (2012).
[18] A. N. Pfeiffer, C. Cirelli, M. Smolarski, R. Dörner, and U. Keller, Nat. Phys. **7**, 428 (2011).
[19] B. Bergues, M. Kübel, N. G. Kling, C. Burger, and M. F. Kling, IEEE J. Sel. Top. Quantum Electron. **21**, 1 (2015).
[20] R. Dorner, T. Weber, M. Weckenbrock, A. Staudte, M. Hattass, R. Moshammer, J. Ullrich, and H. Schmidt-Bocking, Adv. At. Mol. Opt. Phys. **48**, 1 (2002).
[21] W. Becker and H. Rottke, Contemp. Phys. **49**, 199 (2008).
[22] F. Krausz and M. Ivanov, Rev. Mod. Phys. **81**, 163 (2009).
[23] M. Awasthi, Y. V. Vanne, A. Saenz, A. Castro, and P. Decleva, Phys. Rev. A **77**, 063403 (2008).
[24] K. J. Schafer, B. Yang, L. F. DiMauro, and K. C. Kulander, Phys. Rev. Lett. **70**, 1599 (1993).
[25] Q. Liao, A. H. Winney, S. K. Lee, Y. F. Lin, P. Adhikari, and W. Li, Phys. Rev. A **96**, 023401 (2017).
[26] Y. Chen, Y. Zhou, Y. Li, M. Li, P. Lan, and P. Lu, J. Chem. Phys. **144**, 024304 (2016).
[27] C. Huang, W. Guo, Y. Zhou, and Z. Wu, Phys. Rev. A **93**, 013416 (2016).
[28] E. Eremina, X. Liu, H. Rottke, W. Sandner, M. G. Schätzel, A. Dreischuh, G. G. Paulus, H. Walther, R. Moshammer, and J. Ullrich, Phys. Rev. Lett. **92**, 173001 (2004).
[29] C. Guo, M. Li, J. P. Nibarger, and G. N. Gibson, Phys. Rev. A **58**, R4271(R) (1998).
[30] K. Ledingham, R. Singhal, D. Smith, T. McCanny, P. Graham, H. Kilic, W. Peng, S. Wang, A. Langley, P. Taday *et al.*, J. Phys. Chem. A **102**, 3002 (1998).
[31] C. Cornaggia and P. Hering, Phys. Rev. A **62**, 023403 (2000).
[32] V. R. Bhardwaj, D. M. Rayner, D. M. Villeneuve, and P. B. Corkum, Phys. Rev. Lett. **87**, 253003 (2001).
[33] A. S. Alnaser, T. Osipov, E. P. Benis, A. Wech, B. Shan, C. L. Cocke, X.-M. Tong, and C.-D. Lin, Phys. Rev. Lett. **91**, 163002 (2003).
[34] L. Pei and C. Guo, Phys. Rev. A **82**, 021401 (2010).
[35] M. Oppermann, S. J. Weber, L. J. Frasinski, M. Y. Ivanov, and J. P. Marangos, Phys. Rev. A **88**, 043432 (2013).
[36] W. Zuo, S. Ben, H. Lv, L. Zhao, J. Guo, X.-S. Liu, H. Xu, M. Jin, and D. Ding, Phys. Rev. A **93**, 053402 (2016).
[37] A. H. Winney, S. K. Lee, Y. F. Lin, Q. Liao, P. Adhikari, G. Basnayake, H. B. Schlegel, and W. Li, Phys. Rev. Lett. **119**, 123201 (2017).
[38] X. Gong, Q. Song, Q. Ji, K. Lin, H. Pan, J. Ding, H. Zeng, and J. Wu, Phys. Rev. Lett. **114**, 163001 (2015).
[39] A. Zhao, P. Sándor, V. Tagliamonti, S. Matsika, and T. Weinacht, J. Phys. Chem. A **120**, 3233 (2016).
[40] A. Zhao, P. Sándor, and T. Weinacht, J. Chem. Phys. **147**, 013922 (2017).
[41] G. Stibenz, N. Zhavoronkov, and G. Steinmeyer, Opt. Lett. **31**, 274 (2006).
[42] A. T. J. B. Eppink and D. H. Parker, Rev. Sci. Instrum. **68**, 3477 (1997).
[43] A. Zhao, M. van Beuzekom, B. Bouwens, D. Byelov, I. Chakaberia, C. Cheng, E. Maddox, A. Nomerotski, P. Svihra, J. Visser, V. Vrba, and T. Weinacht, Rev. Sci. Instrum. **88**, 113104 (2017).
[44] J. Ullrich, R. Moshammer, A. Dorn, R. Dörner, L. P. H. Schmidt, and H. Schmidt-Böcking, Rep. Prog. Phys. **66**, 1463 (2003).
[45] Note that with the current setup, we cannot convert the electron TOF to longitudinal momentum since the spread in the electron TOF is comparable to the camera's temporal resolution. However, this does not undermine the correlation result shown below since we are only concerned with the momentum component that is either parallel or perpendicular to the laser polarization.
[46] K. Pearson, Proc. R. Soc. London **58**, 240 (1895).
[47] R. L. Wasserstein and N. A. Lazar (unpublished).